Supporting Information for

Assembly and Core Transformation Properties of two Tetrahedral Clusters: $[Fe^{III}_{13}P_8W_{60}O_{227}(OH)_{15}(H_2O)_2]^{30-}$ and $[Fe^{III}_{13}P_8W_{60}O_{224}(OH)_{12}(PO_4)_4]^{33-}$

Pedro I. Molina, Haralampos N. Miras, De-Liang Long and Leroy Cronin*[a]

[a]WestCHEM, School of Chemistry, University of Glasgow, G12 8QQ, UK. E-mail: Lee.Cronin@glasgow.ac.uk; Web: www.croninlab.com

General experimental remarks

Electrochemical experiments. Voltammograms were recorded using a Versastat 4 electro analysis system from Princeton Applied Research. A standard three-electrode cell was used including a Pt mesh counter electrode, a 3 mm glassy carbon working electrode and a Ag/AgCl/KCl (3.0 M) reference electrode operating at room temperature (19 ± 1 ^{o}C). All potentials are quoted relative to the reference electrode. Before performing the experiments, the working electrode (glassy-carbon) was polished with diamond suspensions of decreasing grain size (15 μm, 6 μm and 1 μm) on nylon polishing pads and sonicated first in water and then in methanol after each polishing step. The cell was purged with Ar for at least 15 min before each experiment.

Electro-spray ionisation Mass Spectrometry (ESI-MS). All MS data was collected using a Q-trap, time-of-flight MS (Maxis Impact MS) instrument supplied by Bruker Daltonics Ltd. The detector was a time-of-flight, micro-channel plate detector and all data was processed using the Bruker Daltonics Data Analysis 4.1 software, whilst simulated isotope patterns were investigated using Bruker Isotope Pattern software and Molecular Weight Calculator 6.45. The calibration solution used was Agilent ES tuning mix solution, Recorder No. G2421A, enabling calibration between approximately 100 *m/z* and 3000 *m/z*. This solution was diluted 60:1 with MeCN. Samples were introduced into the MS *via* direct injection at 180 μL h^{-1}. The ion polarity for all MS scans recorded was negative, at 180 ^{o}C, with the voltage of the capillary tip set at 4000 V, end plate offset at –500 V, funnel 1 RF at 300 Vpp and funnel 2 RF at 400 Vpp.

Flame Atomic Absorption Spectrometry (FAAS) and Flame Photometry (FP): W and Fe content (%) was determined by FAAS on a Perkin-Elmer Analyst 400 Atomic Absorption spectrometer. Na content (%) was determined by FP on a Sherwood Scientific M410 INDUSTRIAL Flame Photometer.

Fourier-Transform Infrared (FTIR) Spectroscopy. For FTIR measurements, a few mg of compound was dispersed in a KBr pellet and its spectrum recorded in transmission mode on a JASCO FT-IR 410 spectrometer. Wavenumbers are given in cm^{-1} and intensities are

described as vw = very weak, w = weak, m = medium, s = strong, vs = very strong, sh = sharp or vsh = very sharp.

Nuclear Magnetic Resonance spectroscopy (NMR): ^{31}P NMR spectroscopy was performed on a Bruker Avance III 400 spectrometer on solutions of 50-100 mg of compound in 1 mL of deuterated solvent inside a 5 mm NMR tube. Chemical shifts are referenced to an internal standard (85% H_3PO_4 at 0.00 ppm).

Thermogravimetric Analysis (TGA). Thermogravimetric analysis was performed on a TA Q500 instrument from room temperature to 1000 ^{o}C at heating rate of 5 ^{o}C min^{-1}.

UV-vis spectroscopy (UV-Vis). UV-vis spectra were collected using a Jasco V-670 spectrophotometer in transmission mode using quartz cuvettes with an optical path length of 1.0 cm.

X-Ray Crystallography. X-ray diffraction data for single crystal structure determination was collected on an Oxford Diffraction Gemini Ultra [λ(Mo K_α) = 0.71073 Å] equipped with an ATLAS CCD detector. Corrections for incident and diffracted beam absorption effects were applied *via* analytical numeric absorption correction with a multifaceted crystal model[1] or empirical absorption correction.[2] Structure solution and refinement were performed by using SHELXS-97[3] and SHELXL-97[3] integrated in the WINGX[4] system.

Synthesis and characterization

All reagents were used as purchased without further purification while $Na_{12}[\alpha\text{-}P_2W_{15}O_{56}]\cdot 18H_2O$ was synthesized according to the published procedure.[5]

Synthesis of $Na_{30}[Fe^{III}_{13}P_8W_{60}O_{227}(OH)_{15}(H_2O)_2]\cdot 56H_2O$ (Na_{30}-1):

$FeCl_3\cdot 6H_2O$ (1.0 g, 3.7 mmol) was dissolved in 30 mL of 2 M aqueous NaCl. $Na_{12}[P_2W_{15}O_{56}]\cdot 18H_2O$ (6.0 g, 1.4 mmol) was added to the turbid dark yellow solution in small portions under vigorous stirring over a period of 15 min. This reaction mixture was allowed to stir for a further 5 min before adjusting the pH to 5.00 by dropwise addition of 5 M aqueous NaOH. The dark red limpid solution was heated at 85 °C for 5 min, filtered hot into a wide-neck 100 mL conical flask and finally placed in a temperature-controlled crystallisation room (18 ± 1 °C). Hexagonal dark red plates formed overnight and were isolated from the mother liquor after 3 d. Yield: 1.771 g, 0.10 mmol, 30 % based on W. $Na_{30}[Fe^{III}_{13}P_8W_{60}O_{227}(OH)_{15}(H_2O)_2]\cdot 56H_2O$, $Fe_{13}H_{131}Na_{30}O_{300}P_8W_{60}$, MW = 17626.55 g mol^{-1}. Characteristic IR bands (cm^{-1}): 694 (vs), 795(s), 871 (vs), 900 (s), 938 (sh); 1080 (vs). ^{31}P-NMR (D_2O), δ = -15.5 ppm (85% H_3PO_4, 0.00 ppm). UV absorption: λ(O→M) = 278 nm, ε = 22.14 x 10^4 mol^{-1} L cm^{-1}. Elemental analysis (%) for the dehydrated material $Fe_{13}H_{19}Na_{30}O_{244}P_8W_{60}$, calculated (found): Na, 4.15 (4.22); Fe, 4.37 (4.44); W, 66.38 (66.81). Water content (%), crystallographic (TGA, 25-200 °C, N_2 atmosphere): 5.74 (5.73).

Synthesis of $Na_{33}[Fe^{III}_{13}P_8W_{60}O_{224}(OH)_{12}(PO_4)_4]\cdot 67H_2O$ (Na_{33}-2):

H_3PO_4 (50 µL, 0.73 mmol, 85% wt. in H_2O) was added to 15 mL of 2 M aqueous NaCl followed by $FeCl_3\cdot 6H_2O$ (0.50 g, 1.9 mmol). $Na_{12}[P_2W_{15}O_{56}]\cdot 18H_2O$ (3.0 g, 0.7 mmol) was slowly added over 10 min to the cloudy dark yellow solution under vigorous stirring. The resultant light brown turbid solution was allowed to stir for a further 5 min before carefully adjusting the pH to 5.00 by adding small volumes of first 5 M and then 2.5 M aqueous NaOH. The pH of the brown suspension was maintained between 4.95 and 5.05 for 10 min through dropwise addition of 1 M aqueous NaOH. Thereafter, the reaction mixture was heated at 85 °C for 5 min and the resulting clear dark brown solution was filtered hot and finally placed in a temperature-controlled crystallisation room (18 ± 1 °C). Brown block crystals were isolated from the light brown mother liquor on the following day. Yield: 0.851 g, 0.047 mmol, 28 % based on W. $Na_{33}[Fe^{III}_{13}P_8W_{60}O_{224}(OH)_{12}(PO_4)_4]\cdot 67H_2O$, $Fe_{13}H_{146}Na_{33}O_{319}P_{12}W_{60}$, MW = 18138.53 g mol^{-1}. Characteristic IR bands (cm^{-1}): 696 (vs); 777 (vs), 870 (m), 905 (s), 943 (sh); 956 (s); 1082 (s) . ^{31}P-NMR (D_2O), δ = -16.6 ppm (85% H_3PO_4,

0.0 ppm). UV absorption: λ(O→M) = 280 nm, ε = 21.8 x 10^4 mol^{-1} L cm^{-1}. Elemental analysis (%) for the dehydrated material $Fe_{13}H_{12}Na_{33}O_{252}P_{12}W_{60}$, calculated (found): Na, 4.48 (4.48); Fe, 4.28 (4.25); W, 65.15 (65.24). Water content (%), crystallographic (TGA, 25-200 ^oC, N_2 atmosphere): 6.64 (5.84).

Synthesis of $K_{21}Na_8[KFe_{12}(OH)_{18}(\alpha\text{-}1,2,3\text{-}P_2W_{15}O_{56})_4]$. The pH of 10 mL 0.1 M aqueous KCl was adjusted to 3.0 *via* the addition of a few drops of 0.1 M aqueous HCl. Crystals of Na_{30}-**1** (0.2 g, 0.011 mmol) were added to the stirring solution and the resulting suspension was quickly heated until complete dissolution. The hot yellow solution was filtered at once into a narrow-neck 25 mL conical flask and placed in a temperature-controlled crystallisation room (18 ± 1 ^oC). Yellow block crystals formed overnight and their identity was confirmed as $K_{21}Na_8$-**3** by several unit cell checks. Yield: 0.035 g, 1.9 μmol, 18 % based on W.

Crystal structures

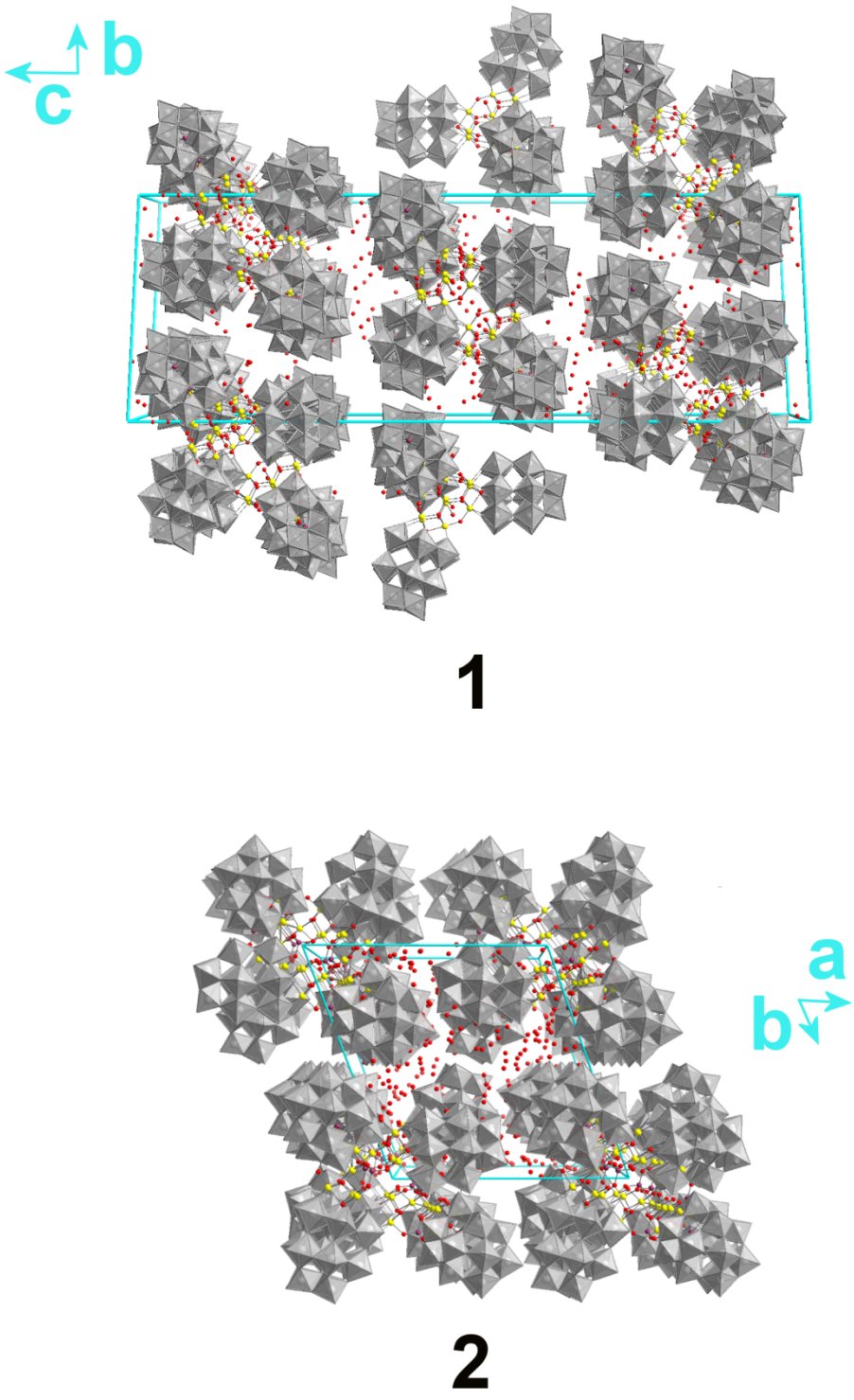

Figure S1. Representations of the crystal structures of Na_{30}-**1** (top) and Na_{33}-**2** (bottom) viewed along the crystallographic *a* and *c* axes respectively. Colour code: WO_6, grey polyhedra; O, red; Fe^{III}, yellow; P, plum. All countercations and some crystallisation waters of crystallisation have been omitted for clarity.

Electrochemistry

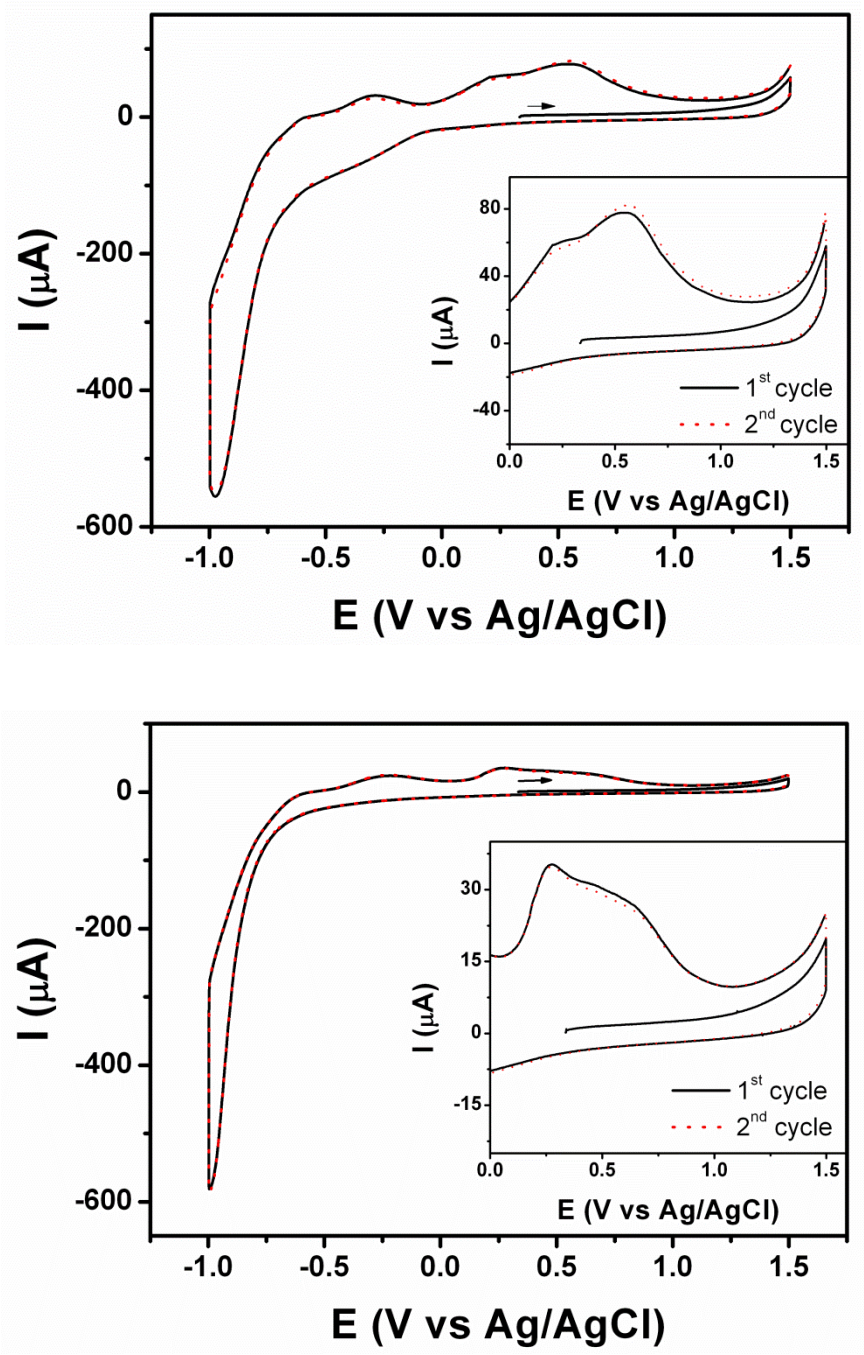

Figure S2. Cyclic voltammograms of **1** (top) and **2** (bottom) solutions at pH = 4.4 ($Na[CH_3COO]/H^+$, 0.1 M; Na_2SO_4, 0.2 M). First (solid black line) and second (dotted red line) cycles obtained at a scan speed of 800 mV s^{-1} are shown. The insets show a magnification of the plot in the anodic region of the voltammogram.

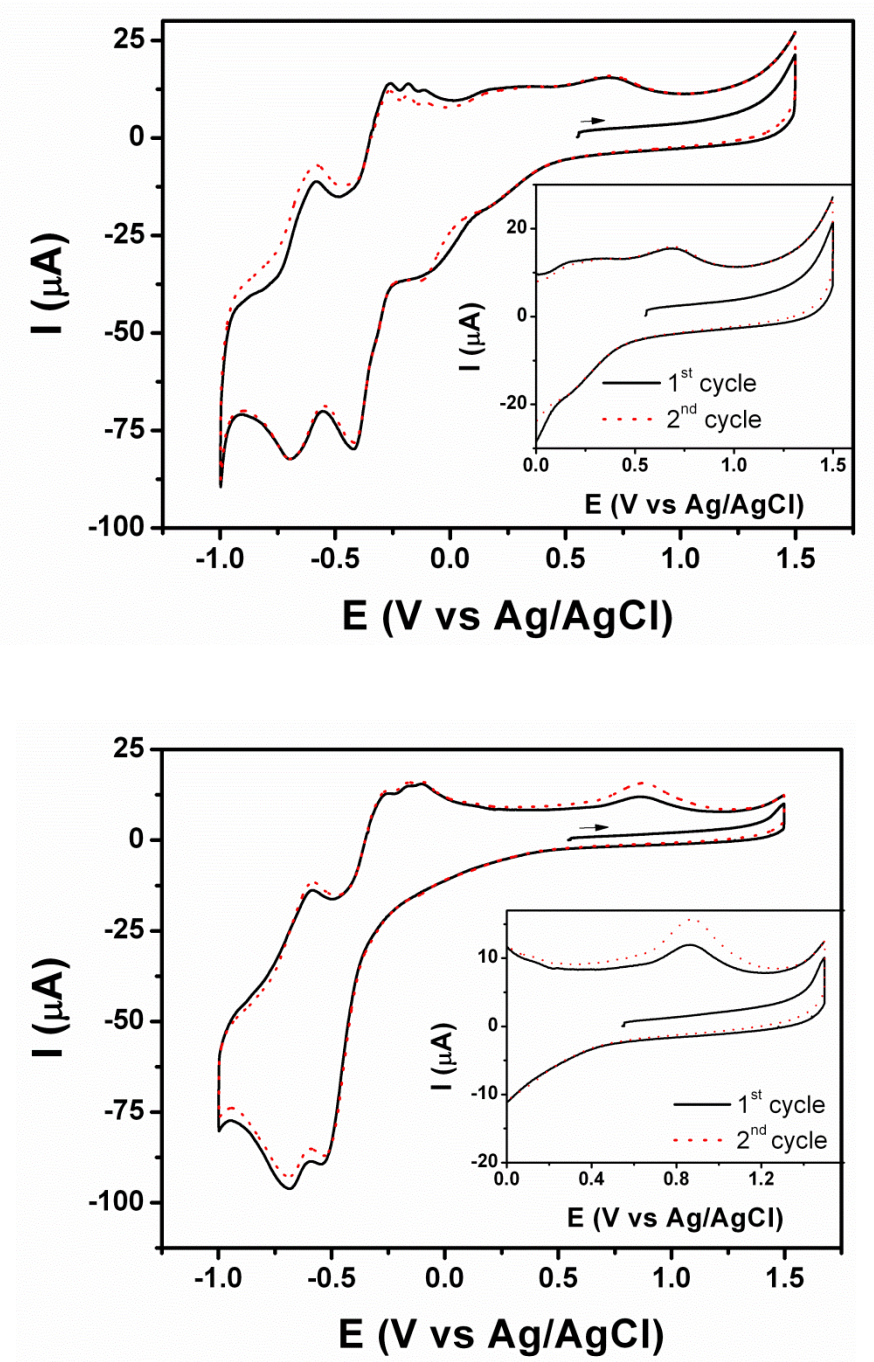

Figure S3. Cyclic voltammograms of **1** (top) and **2** (bottom) solutions at pH = 2.2 (Na_2SO_4/H^+ , 0.2 M). First (solid black line) and second (dotted red line) cycles obtained at a scan speed of 800 mV s^{-1} are shown. Insets show a magnification of the plot in the anodic region of the voltammogram.

FTIR

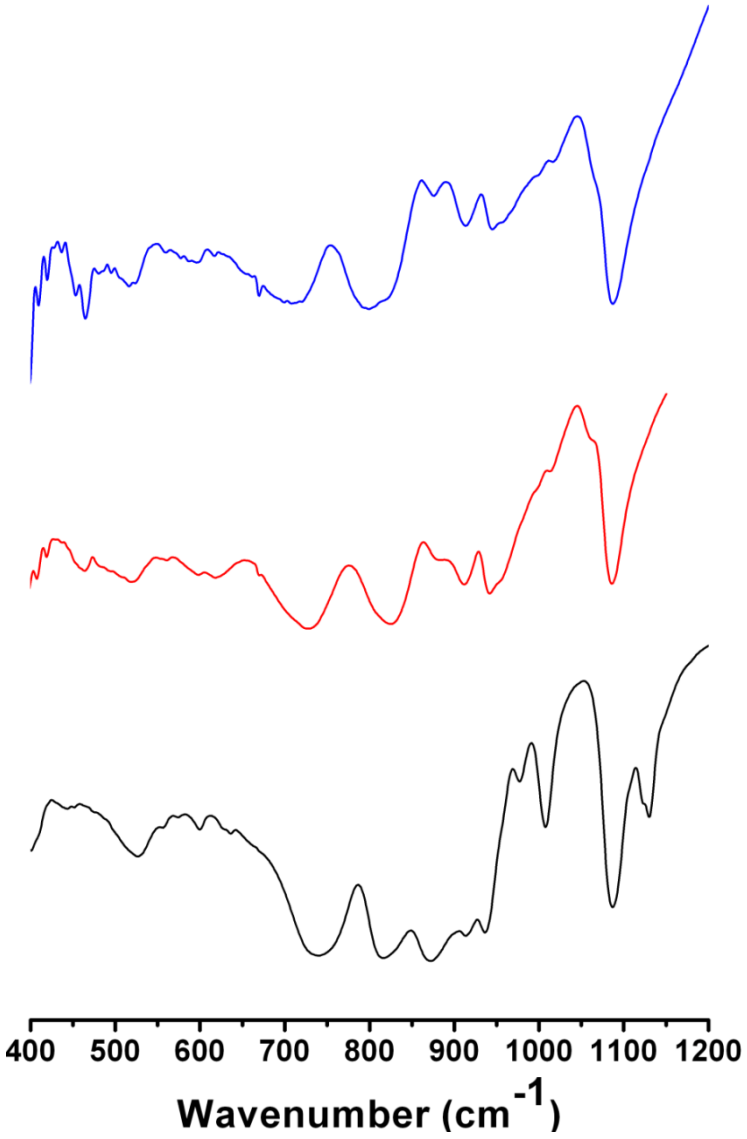

Figure S4. FTIR spectra of Na_{33}-**2** (blue line), Na_{30}-**1** (red line) and $Na_{12}[\alpha\text{-}P_2W_{15}O_{56}]$ (black line). The bands associated to the stretching vibrations of the terminal P-O bond in $\{P_2W_{15}\}$ (1005 and 1131 cm^{-1})[6] are absent in the spectra of Na_{30}-**1** and Na_{33}-**2**.

TGA

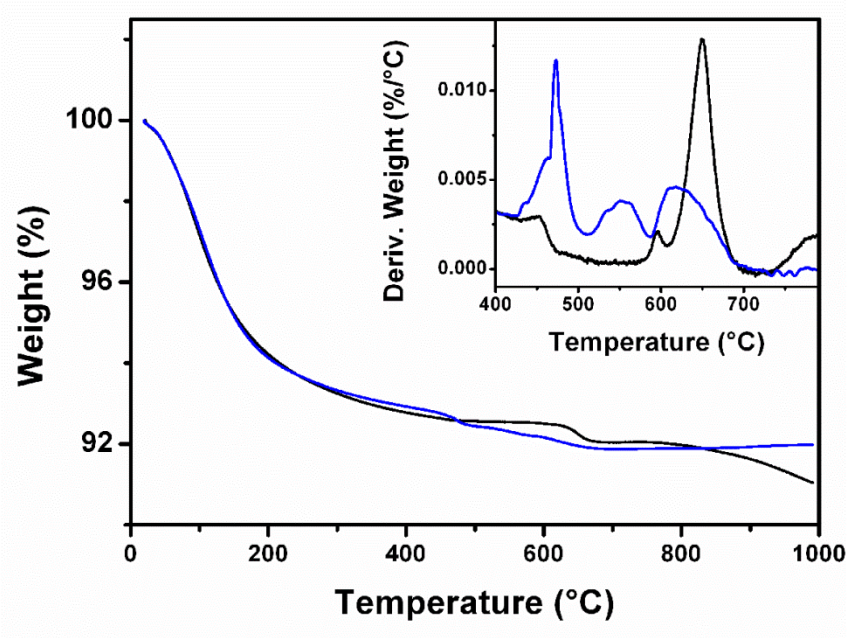

Figure S5. Thermogravimetric analysis (TGA) of Na_{30}-**1** (black line) and Na_{33}-**2** (blue line). Both samples were heated at rate of 5 ^{o}C min^{-1} in a N_2 atmosphere. Inset shows a plot of the ratio of weight change over temperature vs. temperature. The collapse of the cluster framework seems to occur at a lower temperature in Na_{33}-**2** compared to Na_{30}-**1**.

UV-vis

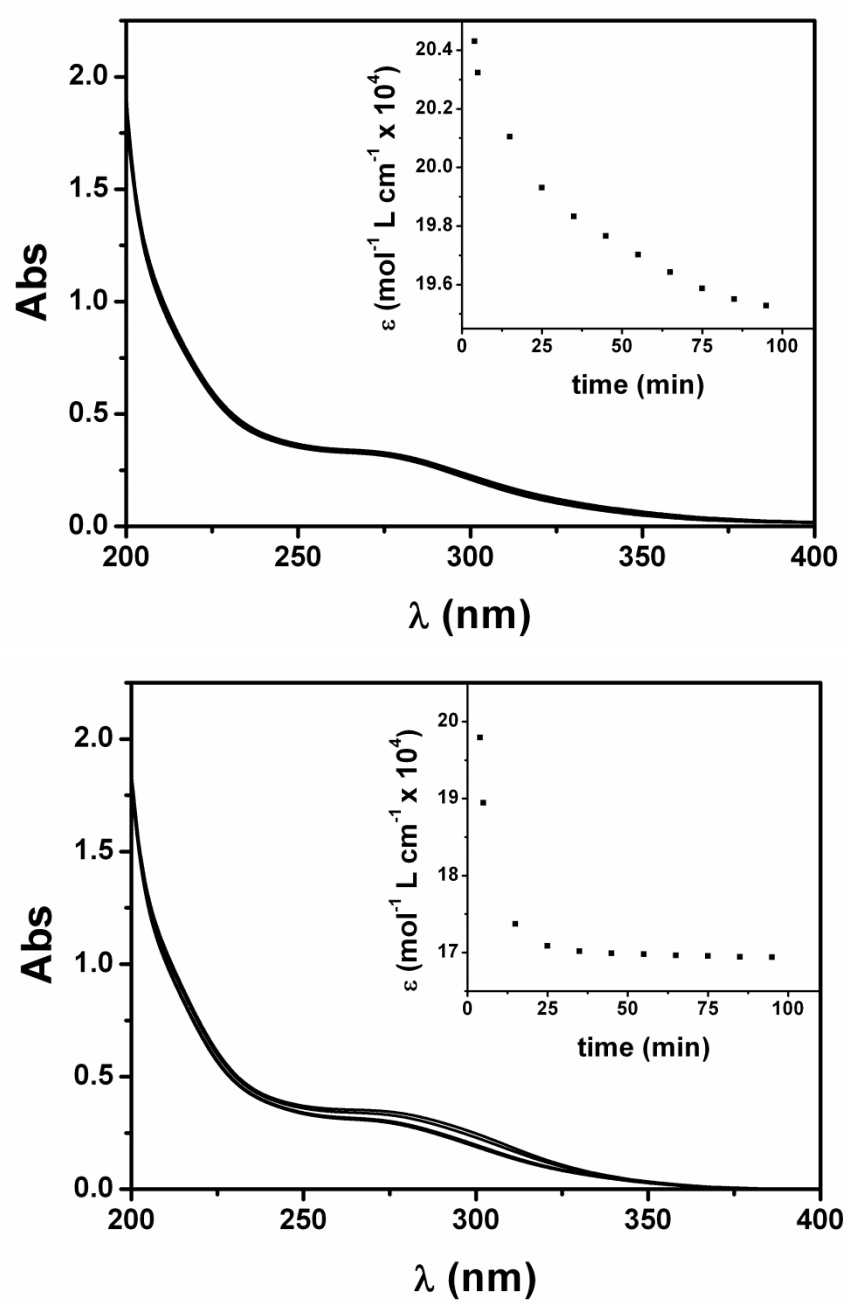

Figure S6. Time profile of UV spectra obtained from solutions of Na_{30}-**1** (top) and Na_{33}-**2** (bottom) in Na_2SO_4/H^+ (0.2 M, pH = 2.2). The insets plot the evolution of the molar absorption coefficient of each cluster at 275 nm with time. According to these measurements, **1** seems to be slightly more stable than **2** in solution.

ESI-MS

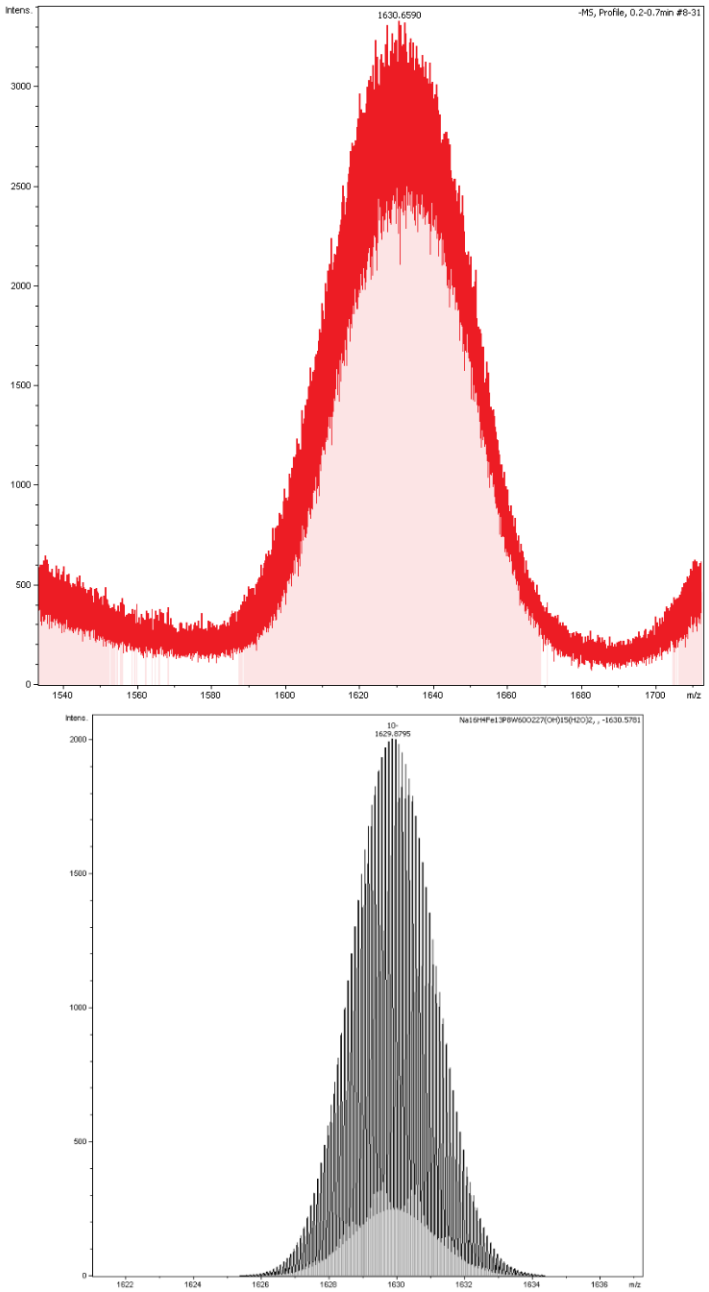

Figure S7. Top, magnification of the mass spectrum shown in Figure 10. Bottom, simulated spectrum for envelope 1 (Table 4).

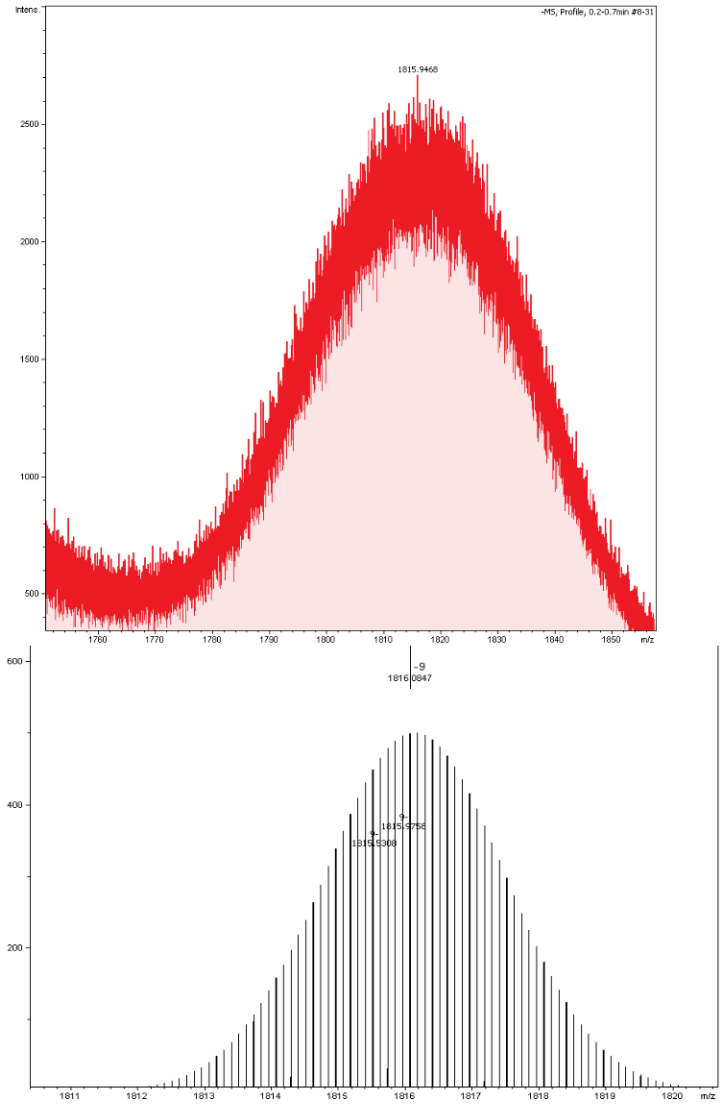

Figure S8. Top, magnification of the mass spectrum shown in Figure 10. Bottom, simulated spectrum for envelope 2 (Table 4).

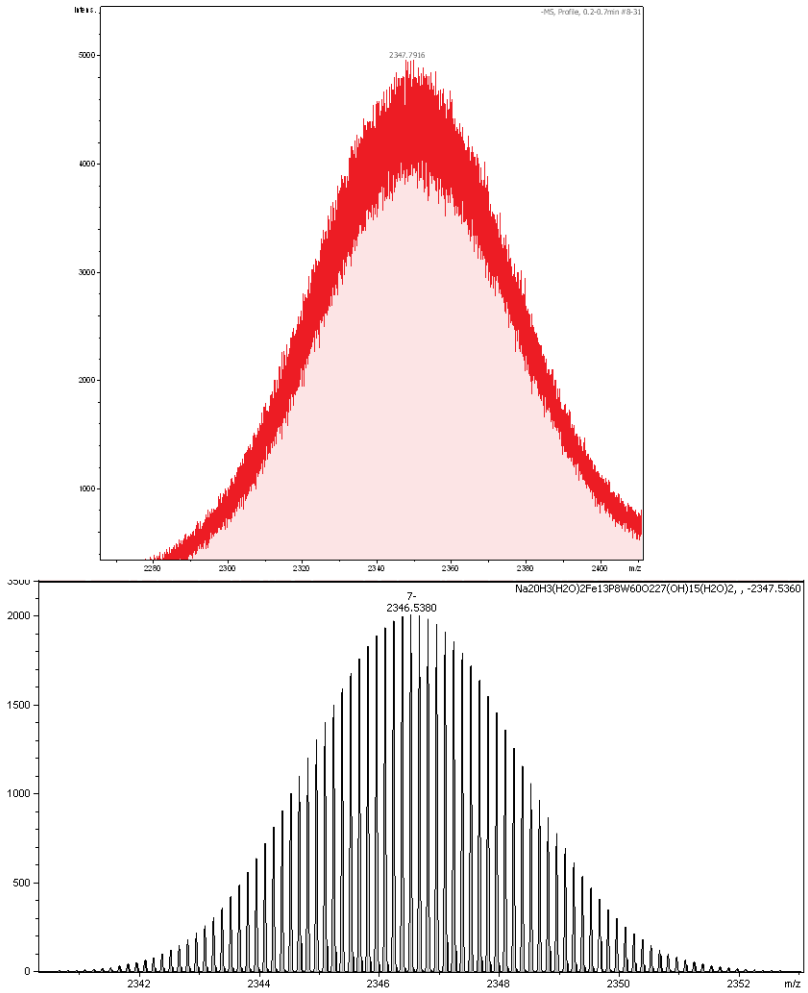

Figure S9. Top, magnification of the mass spectrum shown in Figure 10. Bottom, simulated spectrum for envelope 3 (Table 4).

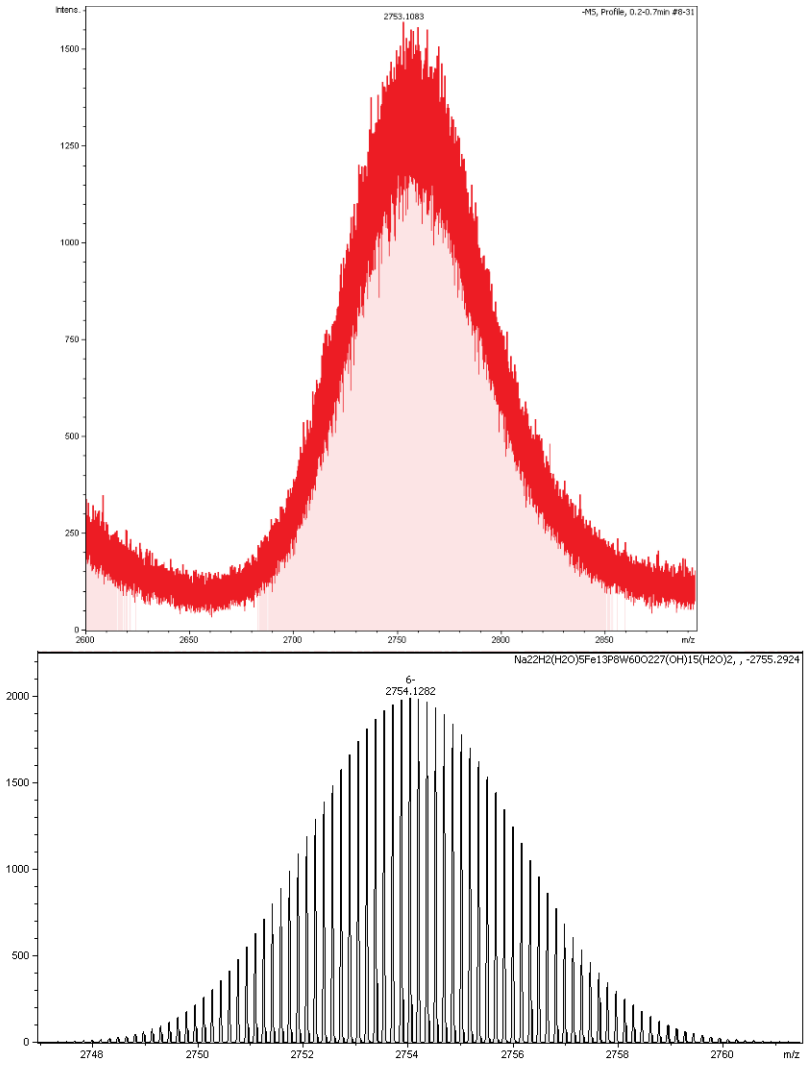

Figure S10. Top, magnification of the mass spectrum shown in Figure 10. Bottom, simulated spectrum for envelope 4 (Table 4).

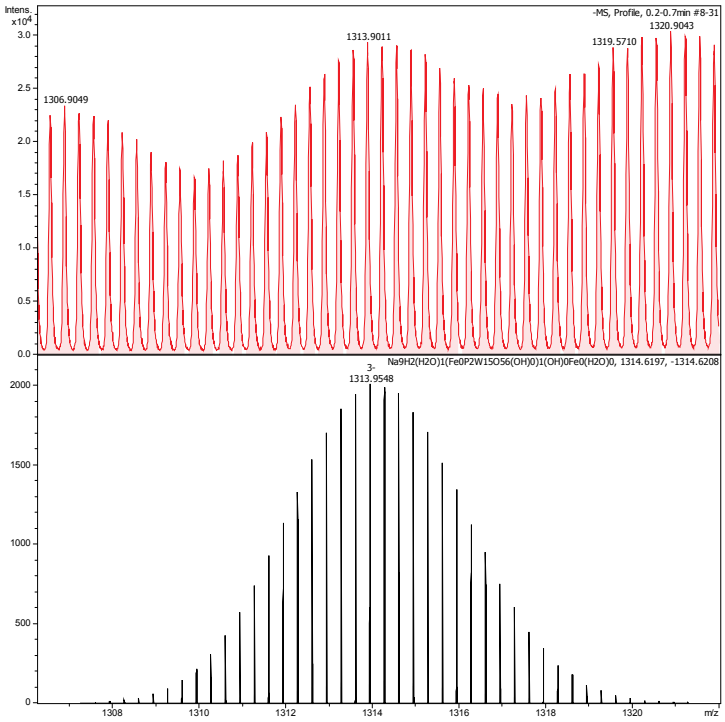

Figure S11. Top, magnification of the mass spectrum shown in Figure 10. Bottom, simulated spectrum for envelope 5 (Table 4).

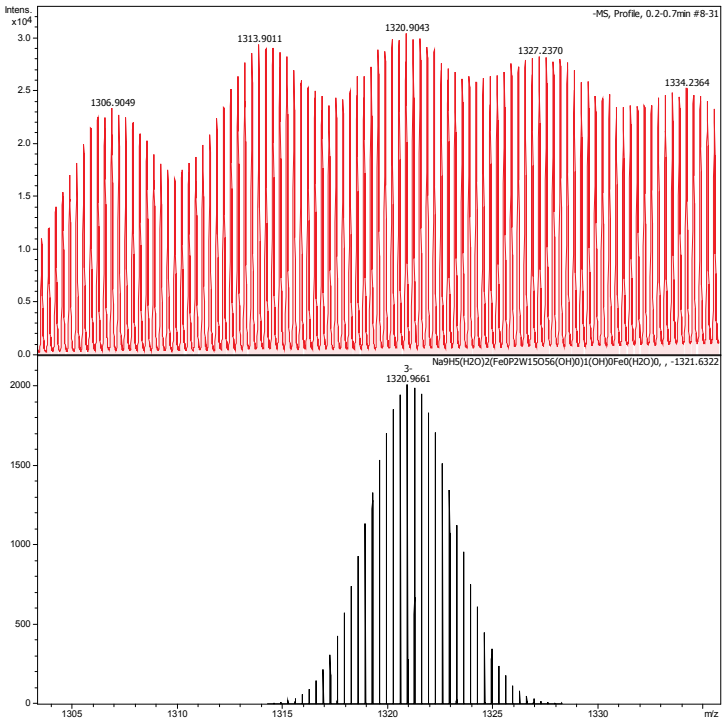

Figure S12. Top, magnification of the mass spectrum shown in Figure 10. Bottom, simulated spectrum for envelope 6 (Table 4).

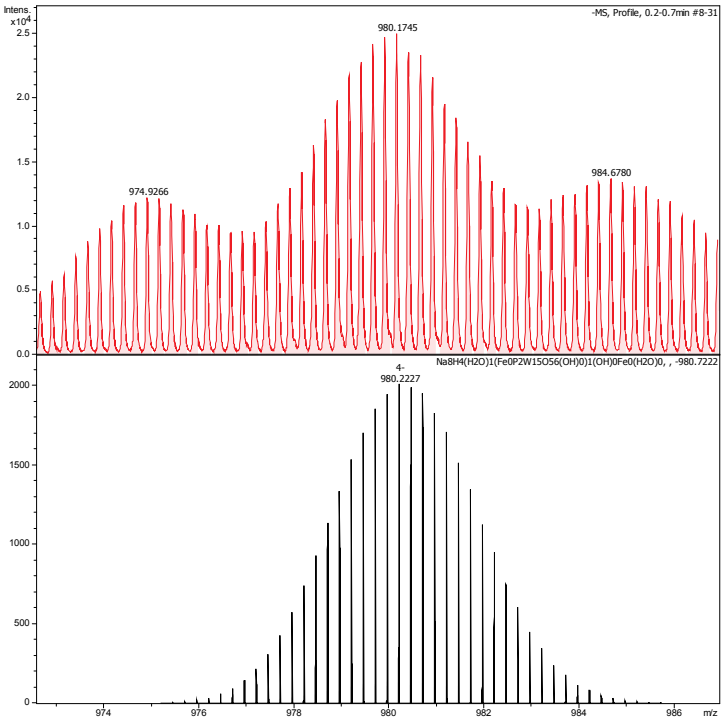

Figure S13. Top, magnification of the mass spectrum shown in Figure 10. Bottom, simulated spectrum for envelope 7 (Table 4).

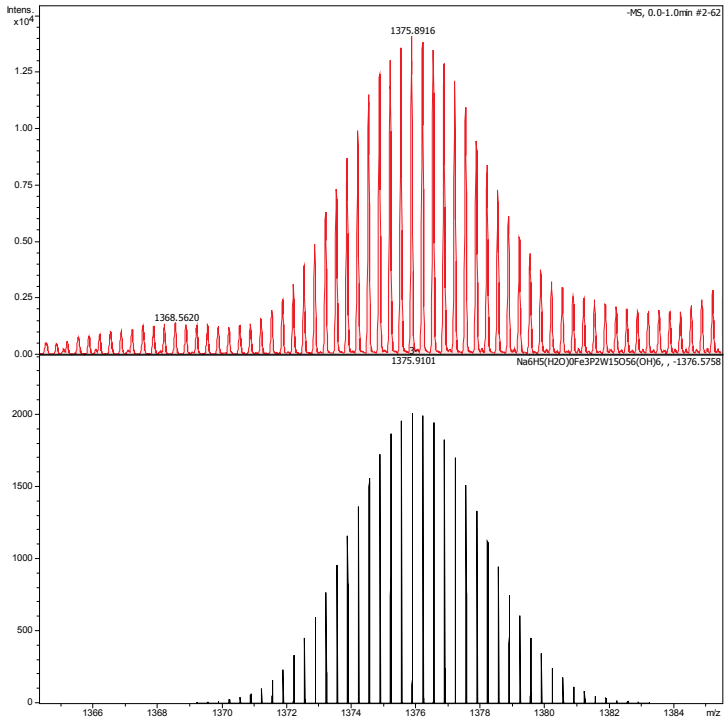

Figure S14. Top, magnification of the mass spectrum shown in Figure 11. Bottom, simulated spectrum for envelope 5 (Table 5).

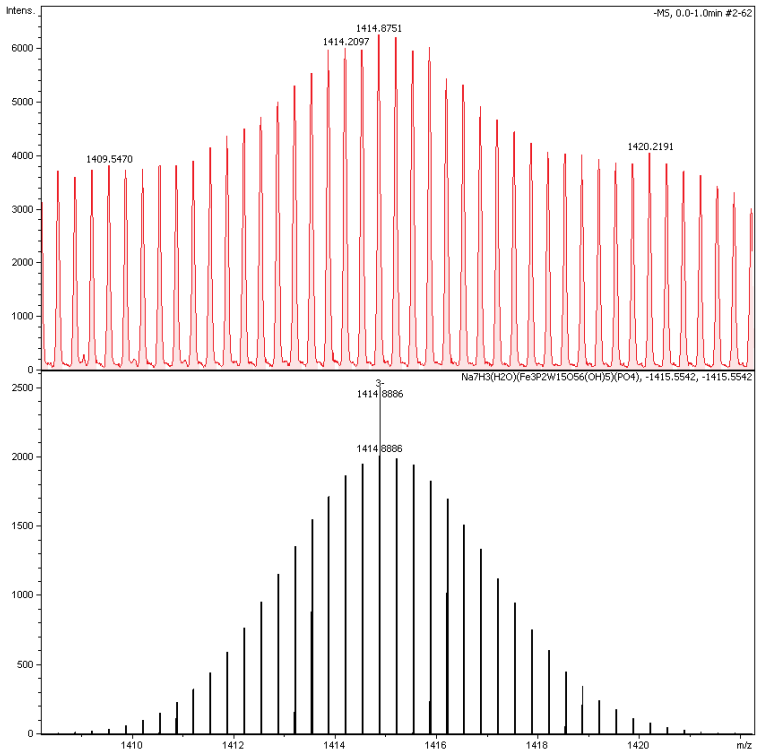

Figure S15. Top, magnification of the mass spectrum shown in Figure 11. Bottom, simulated spectrum for envelope 6 (Table 5).

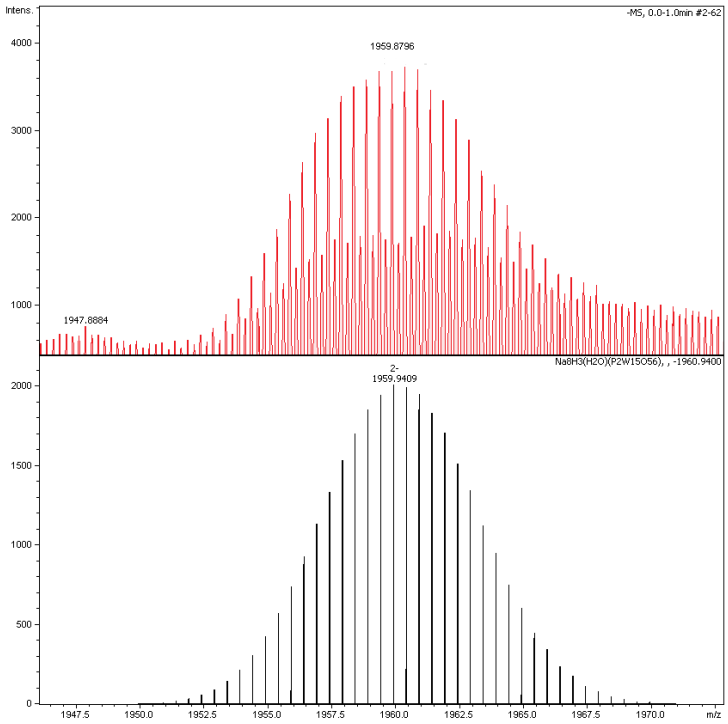

Figure S16. Top, magnification of the mass spectrum shown in Figure 11. Bottom, simulated spectrum for envelope 7 (Table 5).

Bond Valence Summation Analysis (BVS)

Table T1. BVS[7] analysis of the Fe centres in the $\{Fe_3P_2W_{15}\}$ units in **1**.

Atom 1	Atom 2	Distance (Å)	BVS (Fe^{III}/O^{2-})	Assignment
Fe1	O22	1.8779(136)	3.1	Fe^{III}
	O21	1.9640(122)		
	O21	1.9685(105)		
	O19	2.0113(116)		
	O18	2.0157(100)		
	O20	2.2586(91)		
Fe2	O22	1.8775(113)	3.1	Fe^{III}
	O24	1.9676(126)		
	O25	1.9844(108)		
	O28	2.0087(133)		
	O29	2.0248(113)		
	O34	2.2541(112)		
Fe3	O27	1.8933(130)	3.0	Fe^{III}
	O24	1.9682(117)		
	O26	1.9727(100)		
	O30	2.0109(114)		
	O31	2.0148(115)		
	O34	2.2597(128)		
Fe4	O27	1.8748(111)	3.1	Fe^{III}
	O25	1.9722(119)		
	O26	1.9855(120)		
	O33	2.0023(134)		
	O32	2.0067(115)		
	O34	2.2638(109)		

Table T2. BVS analysis of the exolacunary Fe centre in **1**.

Atom 1	Atom 2	Distance (Å)	BVS (Fe^{III}/O^{2-})	BVS (Fe^{II}/O^{2-})	Assignment
Fe5	O25	1.9101(193)	2.5	2.3	Fe^{III}[1]
	O24	1.9233(208)			
	O21	1.9273(147)			
	O23	2.1502(138)			
	O99	2.4256(284)			

Table T3. BVS analysis of the oxo ligands bridging the $\{Fe_3P_2W_{15}\}$ in **1**.

Atom 1	Atom 2	Distance (Å)	BVS (O^{2-}/Fe^{III})	BVS (OH^{-}/Fe^{III})	Assignment
O22	Fe2	1.8775(113)	1.5	1.4	OH^-
	Fe1	1.8779(136)			
O27	Fe4	1.8748(147)	1.4	1.4	OH^-
	Fe3	1.8933(130)			

[1] The absence of a reducing agent in the reaction mixture and the disorder of this crystallographic position supports the assigment of this Fe centre as Fe^{III}.

Table T4. BVS analysis of the oxo ligands coordinated solely to the Fe centres in the $\{Fe_3P_2W_{15}\}$ units of **1**.

Atom 1	Atom 2	Distance (Å)	BVS (O^{2-}/Fe^{III}/Fe^{II})	BVS (OH^-/Fe^{III}/Fe^{II})	Assignment
O21	Fe5	1.9273(147)	1.7	1.7	O^{2-}
	Fe1	1.9640(139)			
	Fe1	1.9685(105)			
O24	Fe5	1.9233(208)	1.7	1.7	O^{2-}
	Fe2	1.9676(126)			
	Fe3	1.9682(117)			
O25	Fe5	1.9101(211)	1.7	1.7	O^{2-}
	Fe4	1.9722(119)			
	Fe2	1.9844(108)			
O26	Fe3	1.9727(100)	1.1	1.1	OH^-
	Fe4	1.9855(120)			

Table T5. BVS analysis of the axial oxo ligands coordinated to the exolacunary Fe centre in **1**.

Atom 1	Atom 2	Distance (Å)	BVS (H_2O/Fe^{II})	BVS (OH^-/Fe^{II})	Assignment
O23	Fe5	2.1502(136)	0.3	0.3	H_2O
O99	Fe5	2.4256(284)	0.2	0.2	H_2O

Table T6. BVS analysis of the Fe centres in the $\{Fe_3P_2W_{15}\}$ units in **2**.

Atom 1	Atom 2	Distance (Å)	BVS (Fe^{III}/O^{2-})	Assignment
Fe1	O189	1.9396(156)	3.1	Fe^{III}
	O163	1.9615(145)		
	O168	1.9760(125)		
	O171	1.9865(134)		
	O172	2.0091(154)		
	O173	2.2446(152)		
Fe2	O247	1.9438(133)	3.1	Fe^{III}
	O165	1.9518(155)		
	O172	1.9624(183)		
	O164	1.9849(142)		
	O170	1.9873(123)		
	O173	2.2683(124)		
Fe3	O242	1.9282(122)	3.1	Fe^{III}
	O167	1.9586(137)		
	O170	1.9684(131)		
	O166	1.9716(176)		
	O171	1.9989(173)		
	O173	2.2410(117)		
Fe4	O169	1.9277(130)	3.1	Fe^{III}
	O104	1.9577(130)		
	O103	1.9624(177)		
	O109	1.9795(172)		
	O110	1.9834(147)		
	O112	2.2640(116)		
Fe5	O241	1.9126(186)	3.1	Fe^{III}
	O240	1.9553(129)		
	O106	1.9651(139)		
	O111	1.9945(147)		
	O109	2.0016(115)		
	O112	2.2639(152)		
Fe6	O251	1.9302(141)	3.1	Fe^{III}
	O108	1.9532(127)		
	O105	1.9810(176)		
	O111	2.0014(179)		
	O110	2.0062(138)		
	O112	2.2154(122)		

Fe7	O249	1.9214(119)	3.2	Fe^{III}
	O44	1.9449(123)		
	O45	1.9639(149)		
	O50	1.9822(187)		
	O49	1.9996(141)		
	O52	2.2623(120)		
Fe8	O96	1.9237(125)	3.1	Fe^{III}
	O46	1.9677(149)		
	O51	1.9789(183)		
	O49	1.9837(141)		
	O47	1.9926(119)		
	O52	2.2632(122)		
Fe9	O248	1.9205(147)	3.2	Fe^{III}
	O48	1.9590(119)		
	O43	1.9681(123)		
	O50	1.9716(139)		
	O51	1.9888(150)		
	O52	2.2480(153)		
Fe10	O243	1.9171(140)	3.2	Fe^{III}
	O227	1.9495(115)		
	O237	1.9685(177)		
	O228	1.9696(152)		
	O238	1.9776(128)		
	O229	2.2520(123)		
Fe11	O246	1.9370(117)	3.1	Fe^{III}
	O223	1.9466(152)		
	O224	1.9490(133)		
	O239	1.9955(189)		
	O238	2.0056(138)		
	O229	2.2223(121)		
Fe12	O252	1.9092(148)	3.2	Fe^{III}
	O225	1.9499(122)		
	O226	1.9608(115)		
	O239	1.9656(158)		
	O237	1.9732(147)		
	O229	2.2798(153)		

Table T7. BVS analysis of the exolacunary Fe centre in **2**.

Atom 1	Atom 2	Distance (Å)	BVS (Fe^{III}/O^{2-})	BVS (Fe^{II}/O^{2-})	Assignment
Fe16	O250	2.0356(184)	2.2	2.2	Fe^{III}[2]
	O109	2.0433(187)			
	O244	2.0489(225)			
	O107	2.0675(160)			
	O111	2.2210(194)			
	O110	2.2620(256)			

[2] The absence of a reducing agent in the reaction mixture and the disorder of this crystallographic position supports the assigment of this Fe centre as Fe^{III}.

Table T8. BVS analysis of the oxo ligands coordinated solely to the Fe centres in the $\{Fe_3P_2W_{15}\}$ units of **2**.

Atom 1	Atom 2	Distance (Å)	BVS (O^{2-}/Fe^{III})	BVS (OH^{-}/Fe^{III})	Assignment
O49	Fe8	1.9837(141)	1.1	1.0	OH^-
	Fe7	1.9996(141)			
O50	Fe9	1.9716(139)	1.1	1.1	OH^-
	Fe7	1.9822(187)			
O51	Fe8	1.9789(183)	1.1	1.0	OH^-
	Fe9	1.9888(150)			
O170	Fe3	1.9684(131)	1.1	1.1	OH^-
	Fe2	1.9873(123)			
O171	Fe1	1.9865(134)	1.1	1.0	OH^-
	Fe3	1.9989(173)			
O172	Fe2	1.9624(183)	1.1	1.0	OH^-
	Fe1	2.0091(154)			
O237	Fe10	1.9685(177)	1.1	1.1	OH^-
	Fe12	1.9732(147)			
O238	Fe10	1.9776(128)	1.1	1.0	OH^-
	Fe11	2.0056(138)			
O239	Fe12	1.9656(158)	1.1	1.1	OH^-
	Fe11	1.9955(189)			

Table T9. BVS analysis of the oxo ligands coordinated to the exolacunary Fe centre in **2**.

Atom 1	Atom 2	Distance (Å)	BVS (O^{2-}/Fe^{III})	BVS (OH^{-}/Fe^{III})	Assignment
O109	Fe4	1.9795(172)	1.5	1.5	OH^{-}
	Fe5	2.0016(115)			
	Fe16	2.0433(187)			
O110	Fe4	1.9834(147)	1.3	1.3	OH^{-}
	Fe6	2.0062(138)			
	Fe16	2.2620(256)			
O111	Fe5	1.9945(147)	1.3	1.3	OH^{-}
	Fe6	2.0014(179)			
	Fe16	2.2210(194)			
O107	P12	1.5542(120)	1.6	1.9	O^{2-}
	Fe16	2.0675(160)			
O244	P9	1.5418(134)	1.7	2.0	O^{2-}
	Fe16	2.0489(225)			
O250	P11	1.5505(167)	1.6	1.9	O^{2-}
	Fe16	2.0356(184)			

Table T10. BVS analysis of the bridging oxo centres forming part of the phosphato ligands in **2**.

Atom 1	Atom 2	Distance (Å)	BVS (O^{2-}/Fe^{III})	BVS (OH^{-}/Fe^{III})	Assignment
O96	P12 Fe8	1.5314(128) 1.9237(125)	1.9	2.2	O^{2-}
O169	P12 Fe4	1.5452(187) 1.9277(130)	1.8	2.1	O^{2-}
O189	P12 Fe1	1.5335(138) 1.9396(156)	1.9	2.1	O^{2-}
O241	P9 Fe5	1.5385(182) 1.9126(186)	1.9	2.2	O^{2-}
O242	P9 Fe3	1.5213(143) 1.9282(122)	1.8	2.2	O^{2-}
O243	P9 Fe10	1.5417(120) 1.9171(140)	1.9	2.1	O^{2-}
O246	P10 Fe11	1.5428(121) 1.9370(117)	1.8	2.1	O^{2-}
O247	P10 Fe2	1.5293(145) 1.9438(133)	1.9	2.2	O^{2-}
O248	P10 Fe9	1.5512(126) 1.9205(147)	1.8	2.1	O^{2-}
O249	P11 Fe7	1.5339(135) 1.9214(119)	1.9	2.2	O^{2-}
O251	P11 Fe6	1.5417(181) 1.9302(141)	1.9	2.1	O^{2-}
O252	P11 Fe12	1.5542(118) 1.9092(148)	1.9	2.1	O^{2-}

References

[1] R. C. Clark and J. S. Reid, *Acta Crystallogr., Sect. A: Found. Crystallogr.*, 1995, **51**, 887-897.

[2] R. H. Blessing, *Acta Crystallogr., Sect. A: Found. Crystallogr.*, 1995, **51**, 33-38.

[3] G. Sheldrick, *Acta Crystallogr., Sect. A: Found. Crystallogr.*, 2008, **64**, 112-122.

[4] L. Farrugia, *J Appl Crystallogr*, 1999, **32**, 837-838.

[5] R. Contant, W.G. Klemperer and O. Yagi, *Inorganic Syntheses*, John Wiley & Sons, Inc., **2007**, pp. 104-111.

[6] P. J. Domaille, G. Hervé and A. Tézé, in *Inorganic Syntheses*, John Wiley & Sons, Inc., **2007**, pp. 96-104.

[7] I. D. Brown, *J. Appl. Cryst.,* **1996**, *29*, 479.